Hierarchical Chiral Luminescent Macrocyclic Porous Organic Polymer from Chiral π-Conjugated Macrocycles: Tunable Circularly Polarized Luminescence and Enantiomeric Fluorescent Sensing

Shiwei Fu,[†,#] Yifan Li,[†,#] Junhao Liang,[†] Qi Wu,[†] Lei Wang,[†] and Yi Liu[†,§*]

[†] Shenzhen Key Laboratory of Polymer Science and Technology, Guangdong Research Center for Interfacial Engineering of Functional Materials, College of Materials Science and Engineering, Shenzhen University, Shenzhen 518060, China.

[§] Center for AIE research, Shenzhen University, Shenzhen 518060, China.

ABSTRACT: Chiral molecules and materials have attracted intense research interest owing to their inherent chiral structure and promising application. Precise synthetic methodologies, novel structures and functions are the core themes during the exploration of chiral materials. Herein, a precise and modular synthetic methodology toward chiral π-conjugated macrocycles (CCMs), combining BINOL moiety with axis chirality and tetraarylethene (TAE) chromophore with helical chirality, are established via intermolecular McMurry coupling. The helical conjugated skeleton within the cyclic skeleton is unambiguously confirmed by single crystal structure. Then, Yamamoto polymerization of the CCMs as monomers feasibly afford a pairs of hierarchical chiral porous organic polymers (POPs) with mirror-imaged chirality. These chiral macrocyclic molecules and chiral macrocyclic POPs all show bright emission as solid state owing to the aggregation-induced emission property of TAE units, and exhibit mirror-imaged circularly polarized luminescence (CPL) with asymmetric factor on the level of 10^{-3}. Accommodation of Rhodamine B as guest molecules into chiral POPs has contributed to color-tunable CPL-active composites via chirality transfer and energy transfer from chiral porous frameworks to non-chiral guests. These chiral luminescent POPs are further utilized to detect explosive molecules via fluorescent quenching, and display enantio-selective sensing of chiral nitro-aromatics. These results have paved a promising platform for fabricating chiral porous materials with AIE function, and will further spur the applications in chiral luminescent POPs.

INTRODUCTION

Porous organic polymers (POPs), featured as a new class of advanced porous materials, have received intense research interests owing to their advantages of inherent porosity, robust scaffolds, high surface areas, tunable structure and tailor-made function.[1,2] Among them, macrocyclic porous organic polymers, are derived from natural-occurring or synthetic macrocyclic compounds as the basic building blocks.[3,4] Relative to common POPs, macrocyclic POPs posse hierarchical porous structures with the combination of inherent cavity from the macrocycles, and extended porous frameworks generated during polymerization.[5] Attributed to this hierarchical porous structure, the host-guest interactions of macrocyclic POPs are further enhanced with well-defined voids. And these macrocyclic porous materials have also shown great potentials in environmental remediation,[6-8] gas adsorption, heterogeneous catalysis,[9,10] fluorescent sensing[11] and ionic conduction[12,13]. Among the reported macrocyclic POPs, conventional macrocyclic compounds, including cyclodextrin,[14] crown ether,[11] calix[4]arene[15] and pillararene,[16] are widely used toward introducing specific supramolecular binding sites into the porous skeleton. The well-established host-guest interaction for these host molecules have been well transplanted into the macrocyclic POPs. In order to endow task-specific functions beyond supramolecular chemistry, functional macrocycles, like porphyrin,[17,18] arylene–ethynylene macrocycles,[19,20] cyclotriveratrylene,[21] and others,[22] are also leveraged to introduce electronic-active or catalytic sites into the functional macrocyclic POPs.

Recently, chiral POPs, including chiral covalent organic frameworks (COFs),[23,24] have gained increasing attentions due to their unique application in enantioselective sensing,[11,25] enantio-separation[26-28] and asymmetric organocatalysis[29-31]. Based on the chiral building blocks with defined point, axis, planar or propeller chirality, 2D chiral porous sheet or 3D chiral porous skeletons are feasibly constructed from irreversible or dynamic covalent chemistry. In the highly crystalline chiral COFs, chiral channels or voids with well-defined chiral environment can be feasibly obtained. However, the structures for chiral cavities in amorphous chiral POPs are usually elusive owing to the lack of long-range order. To introduce precisely defined chiral voids into the amorphous chiral POPs, chiral macrocycles with rigid chiral cavities are promising building blocks, in which the intrinsic chiral voids of macrocyclic compounds can be well retained in chiral macrocyclic POPs. The chiral macrocyclic monomers can correspondingly provide precise bind-
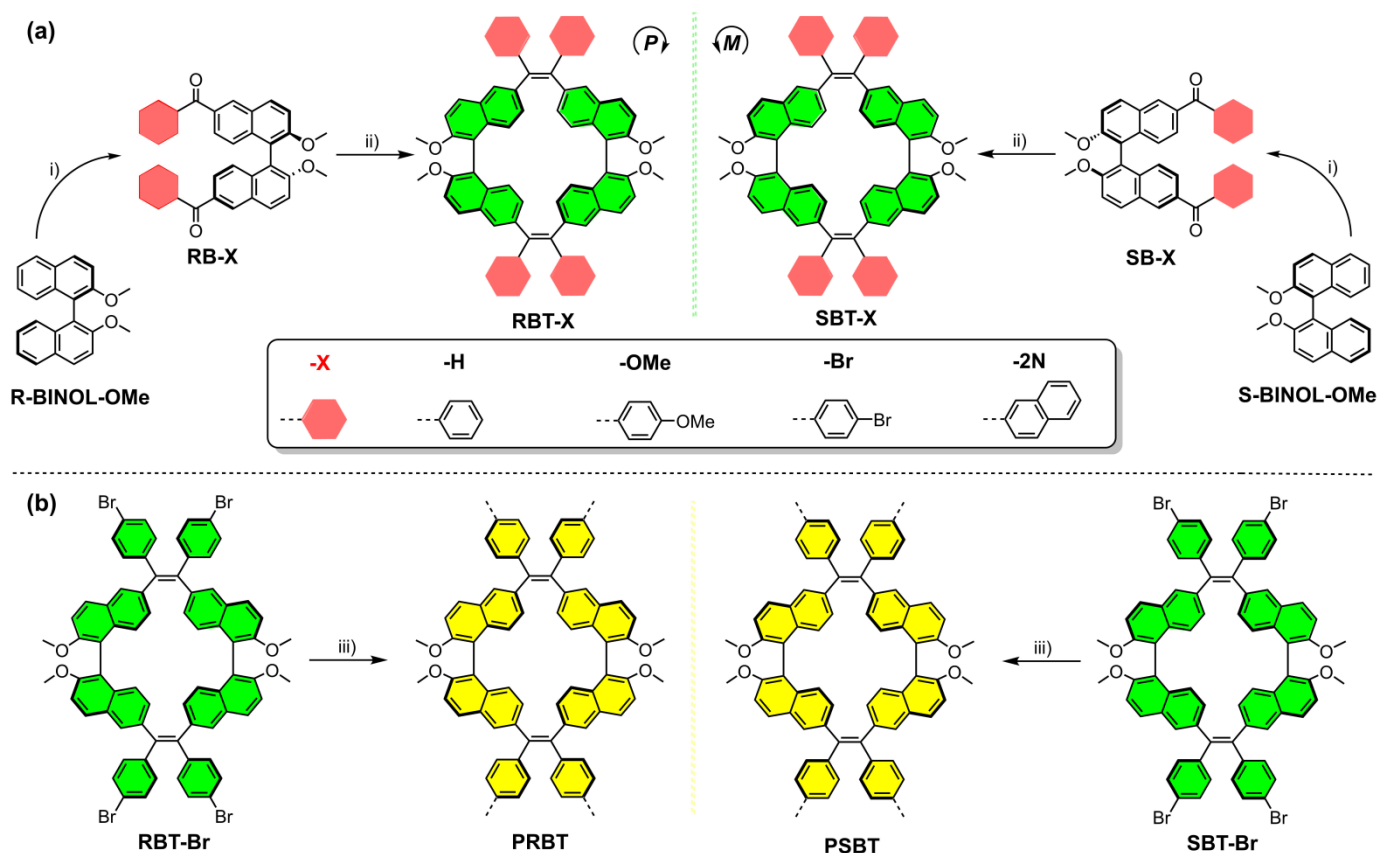
Scheme 1. **(a)** Synthetic routes toward chiral π-conjugated macrocycles **RBT** and **SBT**. (b) Yamamoto polymerization toward chiral macrocyclic POPs. Condition: (i) AlCl₃, benzol chloride, DCM, room temperature, 75.3% for **RB-H**, 59.3% for **RB-Br**, 63.5% for **RB-OMe**, 65.9% for **RB-2N**, 72.7% for **SB-H**, 62.3% for **SB-Br**, 67.5% for **SB-OMe**, 62.1% for **SB-2N**; (ii) TiCl₄, Zn, Pyridine, THF, refluxing, 16.8% for **RBT-H**, 49.4% for **RBT-Br**, 26.4% for **RBT-OMe**, 21.3% for **RBT-2N**, 12.8% for **SBT-H**, 32.9% for **SBT-Br**, 32.2% for **SBT-OMe**, 17.2% for **SBT-2N**; (iii) Ni(COD)₂, COD, Bi-pyridine, Toluene, refluxing, 90% for **PRBT** and 92% for **PSBT**.

ing sites for small guests, and establish functions for further applications.

Chiral macrocycles with defined chiral structures and intriguing porous structure, not only display enantioselective recognition,[32,33] but also engage in other applications related to chirality.[34-36] Among them, luminescent chiral macrocycles embedded with emissive moieties in the chiral cyclic backbone have further proven their potential in enantio-selective fluorescent sensing,[37] circularly polarized luminescence (CPL),[38-41] and chiral organic light emitting diodes (OLED)[42,43]. However, luminescent chiral macrocyclic POPs with hierarchical porous skeleton based on these functional chiral macrocycles are rarely explored owing to their synthetic difficulties. Combing the 3D porous skeleton and luminescent chiral macrocyclic voids, intriguing chiroptical performance and related applications can be evidently anticipated for chiral luminescent macrocyclic POPs.

Herein, we have proposed a module synthetic approach toward chiral conjugated macrocycles (CCMs, denoted as **RBT** and **SBT** in Scheme 1) incorporating both axis and propeller chirality, in which the tetraarylethene (TAE) moiety was embedded via intermolecular McMurry coupling. The helicity of TAE units within the cyclic skeleton was predominated by the commercially available BINOL tethers, and endowed these CCMs aggregation-induced emission (AIE) property with intense emission as solids.

Subsequent Yamamoto coupling of bromide-substituted **RBT** and **SBT** successfully yields a pair of chiral macrocyclic POPs, whereas hierarchical porous skeleton with high surface area around 1000 cm³ g⁻¹ is recorded. These chiral macrocyclic small compounds and POPs all displayed intense emission as aggregates and solids, and exhibited mirror-imaged circularly polarized luminescence (CPL) with asymmetric factor (g_{lum}) on the level of 10^{-3}. Owing to the host-guest interaction between chiral POPs with guest dyes, the CPL emission colors of chiral POPs are further modulated via chirality transfer and energy transfer between chiral POPs and Rhodamines (RB). In addition, these highly luminescent chiral POPs can also detect picric acid via emission quenching, and enantio-selective fluorescence sensing toward chiral nitro-aromatics is also realized.

RESULTS and DISCUSSIONS

Synthesis and structural characterization. Firstly, chiral benzophenone derivatives **RB-X** and **SB-X** were readily obtained via Friedel-Crafts acylation between benzoyl chloride and BINOL moiety with defined axis chirality in presence of AlCl₃ (Scheme 1). Then, the intermolecular McMurry coupling of **RB-X** or **SB-X** could directly yield the macrocycles **RBT-X** and **SBT-X** with satisfactory yield (Scheme 1a). The chemical identities of these chiral macrocycles were firstly confirmed by ¹H nuclear magnet-

ic resonance (NMR) spectroscopy, whereas all proton signals had been unambiguously assigned with the assistance of ^{1}H–^{1}H 2D correlation spectroscopy and nuclear Overhauser effect spectroscopy (Figure S1-S2). In addition, the matrix-assisted laser ionization time-of-flight (MALDI-TOF) mass spectra for **RBT-X** and **SBT-X** also directly indicated the species with desired molar mass, and the experimental isotopic distributions also agreed well with their simulated patterns (Figure S3-S10).

To confirm the chiral skeleton of these CCMs, their single crystals were grown via slow diffusion of Methanol into their solution in tetrahydrofuran (THF). Fortunately, crystals suitable for single crystal analysis had been obtained for **RBT-OMe** and **SBT-OMe** (Figure 1a and 1b, CCDC 2408898 for **RBT-OMe** and CCDC 2408900 for **SBT-OMe**, Table S1). As indicated, the distance between two C=C bond of TAE unit was estimated to be 10.3 Å, whereas the distance between the chiral axis in BINOL moiety was measured to be about 8.3 Å. Notably, the TAE unit within the cyclic skeleton of **RBT-OMe** had adapted the *P*-helicity, whereas their counterparts **SBT-OMe** displayed M-helicity with anticlockwise torsion in TAE core. The chiral transfer between BINOL tethers to TAE units had paved the basis for efficient and precise synthesis toward CCMs.[38,44] The dihedral angle between naphthalene rings within the macrocycle was recorded to be 79° and 97° (Figure 1a), whereas the dihedral angle observed in the crystals of S-BINOL (CCDC 761065) or R-BINOL (CCDC 761061) was 76.6°.[45] This increased angle directly

supported the increased strain within the π-conjugated cyclic skeleton, which driven BINOL moiety far from its pristine structure. Meanwhile, the dihedral angles between naphthalene ring of BINOL with C=C bond in TAE unit were also obviously smaller than the angles between peripheral aryl rings and ethylene linkage (Figure S11-S13). This smaller angle within the cyclic skeleton was also attributed to the constraint from the congested conjugated macrocycles.

Then, a pairs of chiral macrocyclic POP, denoted as **PRBT** and **PSBT**, were successfully obtained via Yamamoto polymerization of **RBT-Br** and **SBT-Br**. The Fourier Transform infrared (FT-IR) spectra of the chiral POP obtained had directly indicated the disappearance of the band at 1064 cm^{-1} (Figure 1d and S14), which corresponded to the asymmetric stretching vibration of C-Br bond.[46] ^{13}C CP-MAS NMR spectra spectra of **PRBT** and **PSBT** were also similar with that of **RBT-H** and **SBT-H** (Figure S15), indicating their similar structure. Scanning electronic microscopy (SEM) results verified the sphere-like morphology for these chiral POPs (Figure S14), whereas X-ray diffraction curves directly supported their amorphous nature (Figure S16). Energy dispersive spectrometer (EDS) analysis of these POP samples suggested their compositions (Figure S17-S18, Table S2-S3), whereas no residual Ni had been recorded. Thermogravimetric analysis (TGA) further indicated their high thermal stability with decomposition temperature up to 420 °C (Figure S19).

To confirm the hierarchical porous structure of these
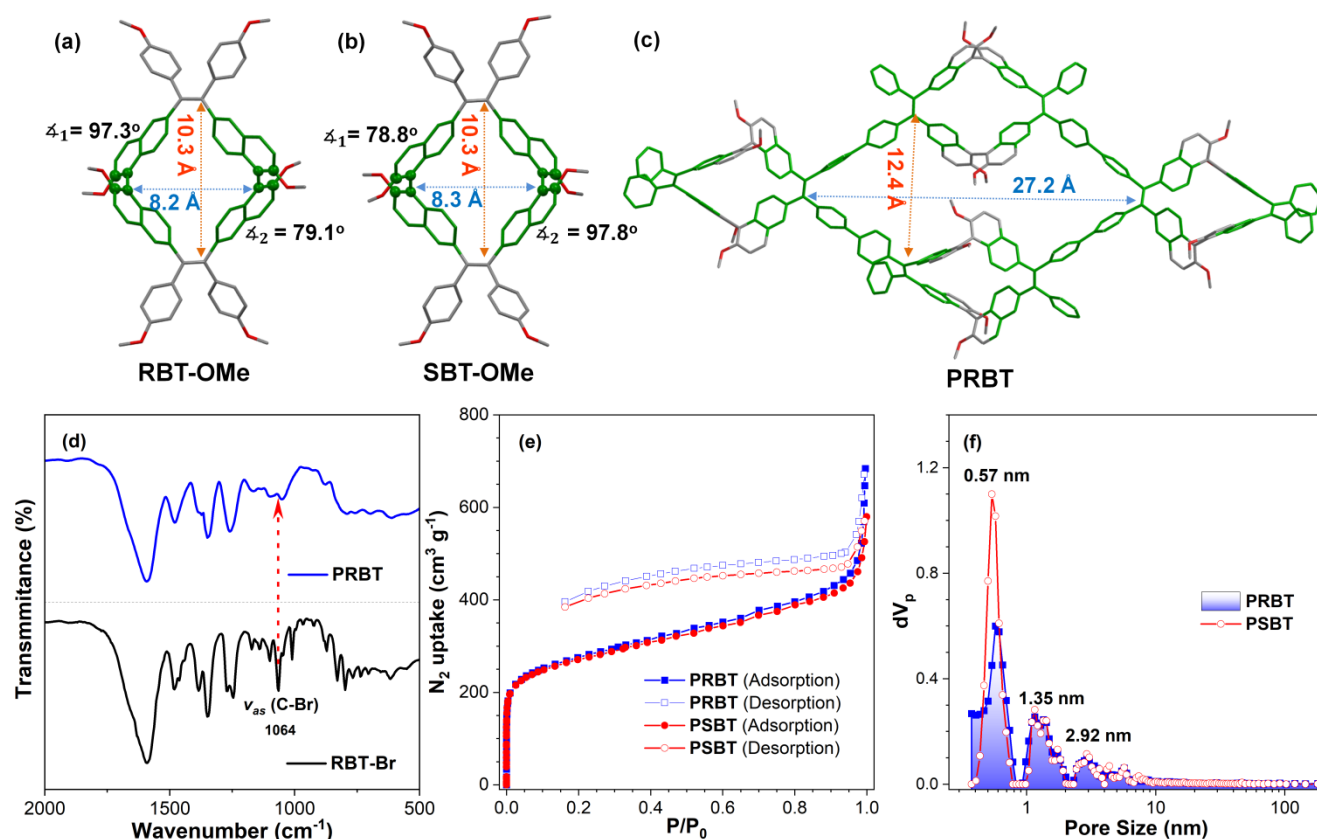
Figure 1. Single crystal structures for chiral π-conjugated macrocycles **RBT-OMe** (a) and **SBT-OMe** (b). (c) Optimized structure for the substructures of chiral POPs **PRBT**. (d) FT-IR spectra of **RBT-Br** and **PRBT**. (e) BET curves and (f) pore distributions for **PRBT** and **PSBT**.

two chiral macrocyclic POPs, their inherent pore structure and distribution were further investigated via the adsorption and desorption of N_2 (Figure 1e and S20). The Brunauer–Emmett–Teller (BET) surface areas of **PRBT** and **PSBT** was recorded to be approximately 1007 m^2 g^{-1} and 992 m^2 g^{-1}, respectively. And the pore size distribution profiles for chiral POPs revealed the presence of micropores with a size of about 0.57 nm, 1.35 nm and 2.92 nm (Figure 1f), whereas the small cavity was attributed to the intrinsic pore of the CCMs and the larger voids were originated from the three-dimensional scaffold (Figure 1c).

This multiple-modal pore size distribution directly con-

firmed the hierarchical porous structures of **PRBT** and **PSBT**, in which the chiral voids within CCM unit had been well retained in chiral macrocyclic POPs.

Aggregation-induced emission. To explore the photo-physical properties of the chiral macrocycles and corresponding chiral POPs, the UV-vis absorption spectra of these chiral materials were firstly recorded (Table S4). The chiral macrocycles with diverse substitutions exhibited similar absorption maximal around 363 nm (Figure 2a), and the optical band gap (E_{opt}) for these compounds was estimated to be 3.04 eV for **SBT-H**, 3.0 eV for **SBT-Br**, 2.96 eV for **SBT-OMe**, and 2.93 eV for **SBT-2N** in THF
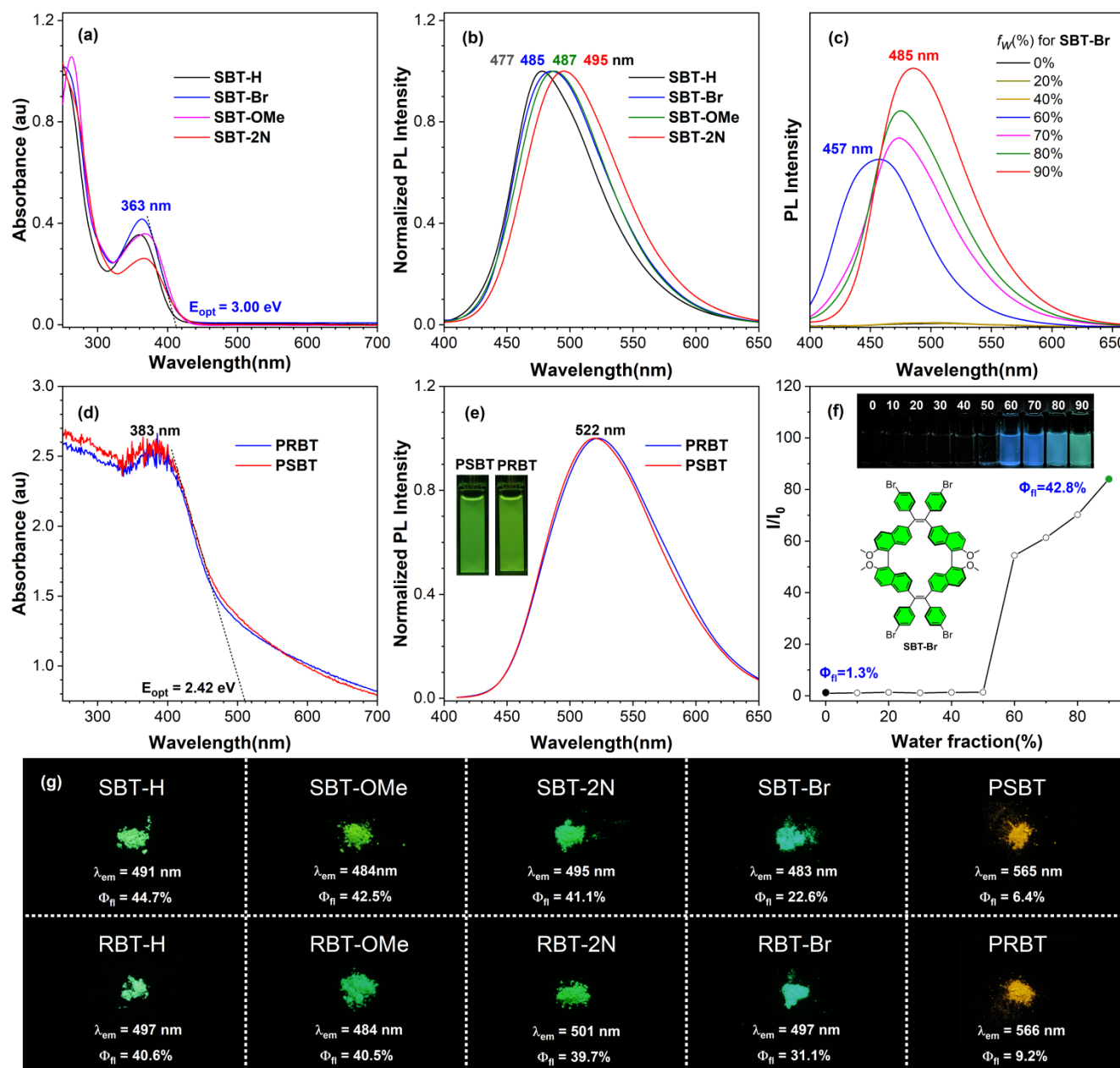
Figure 2. (a) UV-vis absorption spectra of chiral π-conjugated macrocycles in THF. (b) PL spectra of the chiral macrocycles in THF-H2O (1/9). (c) PL spectra of **SBT-Br** in the mixture of THF and water. (d) UV-vis absorption spectra and (e) PL spectra for the suspensions of chiral POPs in MeOH. (f) Dependence of emission intensity (I) for **SBT-Br** on the water fraction 1of THF-water mixture, inset: images of **SBT-Br** solution with different water content under UV lamp. (g) Images of chiral π-conjugated macrocycles and chiral POPs as solid sample under UV lamp, labeled with their emission wavelength and efficiency as powder. Concentration: 10 uM for chiral macrocycles, 10 uM for the repeating unit of chiral POPs. Excitation wavelength: 380 nm for **RBT** and **SBT**, 390 nm for **PRBT** and **PSBT**.

(Figure 2a). This trend was well consistent with the simulated band gap for these series of chiral macrocycles based on DFT calculation on the basis set of b3lyp/6-31G(d), in which the band gap gradually decreased from 3.51 eV for **SBT-H** and 3.45 eV for **SBT-Br**, to 3.41 eV for **SBT-OMe** and 3.30 eV for **SBT-2N** (Figure S21-S23). By contrast, the chiral POPs **PRBT** and **PSBT** exhibited obviously red-shifted absorption band at 383 nm relative to their monomers, whereas the E_{opt} had also decreased to 2.42 eV owing to the extended π-conjugation (Figure 2d)[46].

Owing to the existence of tetraarylethene (TAE) moiety in the chiral macrocycle, the aggregation-induced emission properties and solid-state emission for these chiral materials were further studied (Figure S24-S31). For conjugated macrocycles, they displayed classical AIE behavior with low emission intensity in THF and intense emission as nano-aggregates. Under low water content (f_w), these CCMs displayed very weak emission, for example, the absolute emission quantum yield (ϕ_F) for **SBT-OMe** and **SBT-Br** was recorded to be as low as 1.5% and 1.3% in pure THF. When the water content exceeded a threshold value, the emission intensity and lifetime of these CCMs dramatically raised owing to the formation of nano-aggregates (Figure 2f and S32). For instance, the ϕ_F for **SBT-OMe** and **SBT-Br** had increased to 42.1% and 42.8% in THF-H_2O mixture (1/9). Interestingly, the emission wavelength for **SBT-Br** had obviously blue-shifted to 457 nm under $f_w = 60\%$, relative to the green emission at 485 nm when $f_w = 90\%$. This blue-shifted emission was proba-

bly attributed to the formation of nano-crystals, which had been widely observed in the mechano-chromic luminescence for AIEgens.[47,48] Notably, these four pairs of chiral macrocycles all exhibited bright blue or green emission with high ϕ_F in solid state, as nano-aggregates, and in PMMA film as shown in Figure 2g and Table S4.

By contrast, the two chiral POPs **PRBT** and **PSBT** displayed distinguished yellow green emission at 522 nm as a suspension in MeOH and orange emission at 565 nm as powder (Figure 2e and 2g), whereas the red-shifted emission was attributed to the extended π-conjugation in the 3D porous scaffold[46]. And the absolute ϕ_F for **PRBT** and **PSBT** were measured to be 18.4% and 17.1% as suspension in MeOH, and 9.2% and 6.4% as powder, respectively (Figure S33). This was obviously lower than that of the chiral macrocycles in both states. The attenuated emission efficiency for luminescent POPs was probably owing to the free rotation of phenyl rings in the 3D porous shape-persistent scaffold.

Circularly polarized luminescence. Owing to the stable helical cyclic skeleton within these chiral macrocycles, their electronic circular dichroism (CD) and CPL spectra were further explored. As shown in Figure 3a, these four pairs of chiral macrocyclic AIEgens all exhibited strong and fully mirror-symmetric CD signals which indicated their enantiomeric structures. In pure THF, the chiral macrocycles **RBT** all showed strong negative first Cotton effects around 378 nm, while **SBT** exhibited positive
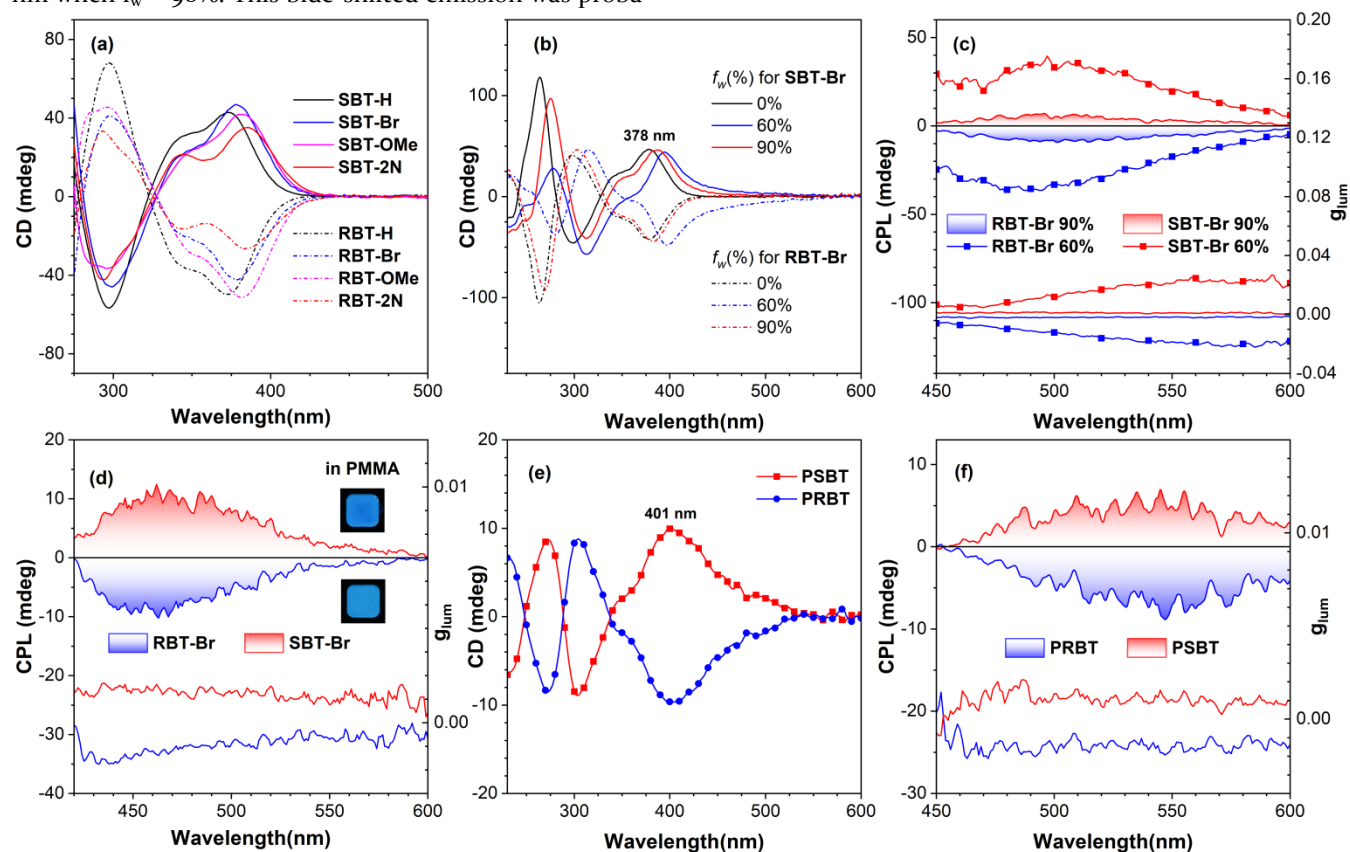
Figure 3. (a) CD spectra of chiral π-conjugated macrocycles **SBT** and **RBT** in THF. (b) CD spectra of **SBT-Br** and **RBT-Br** in THF and THF-H_2O mixture. (c) CPL spectra and g_{lum} values of **SBT-Br** and **RBT-Br** in the THF-H_2O (4/6 and 1/9) mixture. (d) CPL spectra of **SBT-Br** and **RBT-Br** in the PMMA film (1% w/w). (e) CD and (f) CPL spectra of **PSBT** and **PRBT** in MeOH. Concentration: 10 uM for chiral macrocycles, and 10 uM for the repeating unit of chiral POPs. Excitation wavelength: 360 nm for **RBT** and **SBT**, 390 nm for **PRBT** and **PSBT**.

ones. The identical CD bands of all **RBT** and **SBT** series indicated their similar chiral skeleton relative to **RBT-OMe** and **SBT-OMe**. And thus, the TAE units within **RBT** were all in *P*-configuration, whereas TAE moiety in **SBT** all adopted the *M*-helicity.[49] In addition, the first cotton band around 380 nm also slightly res-shifted from **R/SBT-H** to **R/SBT-2N**, which also agreed well with the decreased E_{opt} observed in UV-vis absorption curve. The CD bands of these CCMs also agreed well with their simulated CD spectra based on time-dependent (TD) DFT calculations (Figure S34).

Then, CD spectra of **RBT** and **SBT** in the THF-H₂O mixture were further studied to evaluate the impacts of aggregates formation on their chiral-optical properties. As shown in Figure 3b and Figure S35, although the CD band had slightly shifted parallel with the aggregates formation, the CD intensity and sign was nearly independent on the formation of nano-aggregates. This was different from the aggregation-induced CD annihilation phenomenon observed for chiral small molecules and polymers derived from BINOL moieties.[50] For most derivatives of BINOL, the changing dihedral angle between two naphthyl rings would contribute to the annihilation of CD signals after aggregates formation. This remarkable distinction had strongly supported the shape-persistent skeleton of these CCMs, in which the dihedral angles within BINOL were highly constrained owing to the conjugated macrocyclic skeleton.

For chiral POPs, the sign of CD spectra for **PRBT** and

PSBT was consistent with that of their monomers, whereas **PRBT** showed a strong negative first Cotton effect and **PSBT** exhibited a positive one. However, their first CD band had obviously red shifted from 378 nm for **RBT-Br** in THF to 401 nm (Figure 3e), which was also consistent with the red-shifted absorption of POPs originated from the extended π-conjugation in the 3D polymeric scaffold.

Owing to the defined helicity of these chiral macrocycles, the chiral AIEgens **RBT** with *P*-configuration all displayed right-handed CPL emission with negative signals as nano-aggregates in THF-H₂O (1/9), whereas **SBT** all exhibited left-handed CPL emission with positive signals (Figure 3c, and S36-S39). The CPL sign of these chiral AIEgens were well consistent with the reported chiral TPE derivatives.[38,44] The corresponding g_{lum} values for **RBTs** as nano-aggregates were about -2.17×10^{-3} for **RBT-H**, -1.85×10^{-3} for **RBT-Br**, -1.45×10^{-3} for **RBT-OMe**, and -1.13×10^{-3} for **RBT-2N**, respectively (Table S5). Surprisingly, the g_{lum} for nano-aggregates of **RBT-Br** and **SBT-Br** in THF-H2O (4/6) had been greatly amplified to -6.69×10^{-3} and 5.25×10^{-3} (Figure S40). This was probably owing to the long-range ordered arrangement of chiral AIEgens in nano-crystals.[51]

In the PMMA film, these enantiomers also emitted CPL signals with the same CPL sense and similar g_{lum} values when compared to the nano-aggregates in THF-H₂O (1/9) (Figure S41-S44). This indicated that there was no supramolecular ordered self-assembly of these CCMs in the PMMA matrix, which would lead to amplified CPL signals.
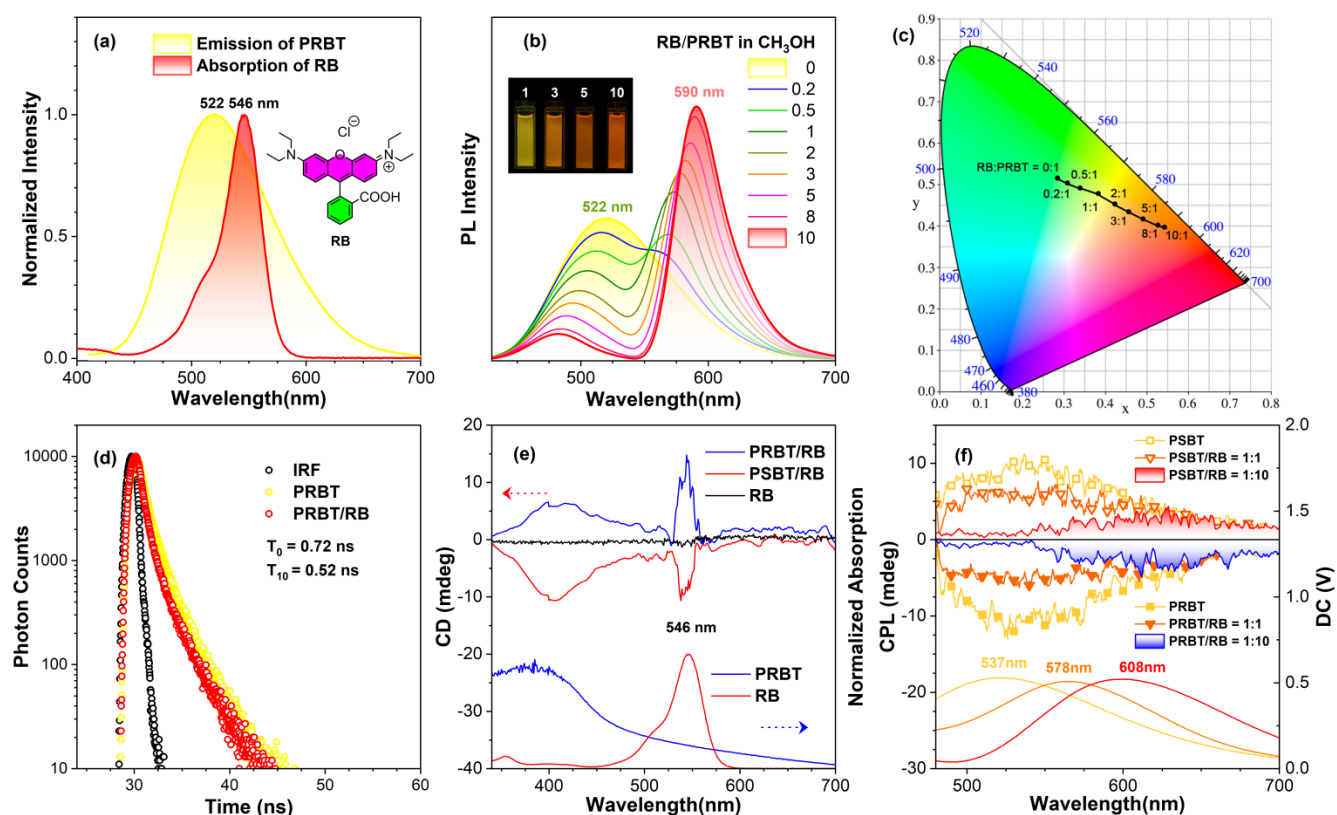
Figure 4. (a) PL spectra of chiral POP **PRBT** as donor and UV-vis absorption spectra of **RB** as acceptor in MeOH. (b) PL spectra of **PRBT** in presence of **RB** in MeOH. (c) CIE color coordinates for the mixture of **PRBT** and **RB**. (d) Luminescence lifetime decay of **PRBT** in absence and presence of **RB** in MeOH. (e) UV-vis absorption and CD spectra of **RB**, **PRBT/RB**, and **PSBT/RB** in MeOH. (f) CPL spectra of **PRBT** and **PSBT** in presence of **RB** in MeOH. Concentration: 10 uM for the repeating unit of chiral POPs. Excitation wavelength: 390 nm for **PRBT** and **PSBT**.

And relative to that as nano-aggregates, the PL maximal in PMMA matrix also obviously blue-shifted probably owing to the congested conformation of these CCMs under constrains of PMMA chains (Figure S45).[38,52] In addition, the chiral POPs also displayed yellow CPL signal with consistent sense and comparable g_{lum} as suspension in MeOH, whereas both **PRBT** and **PSBT** exhibited CPL at 540 nm with $|g_{lum}|$ of approximately 10^{-3} (Figure S46). This result agreed well the amorphous nature of these chiral POPs, which was in contrast with the amplified CPL signals in previously reported chiral crystalline COFs.[53]

CPL modulation via guest dyes. For porous organic polymers, their capability to accommodate small molecules had paved the foundation for their applications in gas capture and fluorescent sensing.[5] Regarding the CPL property of **PRBT** and **PSBT**, the potential host-guest binding would also facilitate the modulation of their CPL performance. Herein, Rhodamine B (RB) was selected as the guest dye to construct tunable CPL materials. As shown in Figure 4a, the absorption spectra of RB with maximal absorption at 547 nm were mostly overlapped with the PL spectra of **PRBT** and **PSBT** with maximal emission at 522nm. Concerning this spectra overlap, fluorescence resonance energy transfer (FRET) from chiral POPs as donors to RB as acceptors was possible when the guest RB was accommodated into the chiral porous skeleton.

Parallel with the addition of RB into the suspension of **PRBT** or **PSBT** in MeOH, the PL intensity at 522 nm which originated from chiral POPs gradually decreased along with the elevated emission at 594 nm from RB (Figure 4b and S47). The CIE color coordinates of **PRBT** had gradually shifted from (0.28, 0.51) for pure PRBT to (0.54, 0.40) for their complex (PRBT/RB = 1/10) (Figure 4c and S48). Luminescent decay curves had indicated that the lifetime of **PRBT** had decreased from 0.72 ns in absence of **RB** to 0.52 ns after addition of 100 uM RB into the mixture (Figure 4d and S49). This lifetime decrease had supported the energy transfer process from chiral POPs as donors to **RB** as acceptor.

In addition, CD spectra of **PRBT** and **PSBT** in presence of **RB** were also measured (Figure 4e and S50). Obviously, a new cotton bond at 546 nm had appeared after the addition of **RB**, which was probably attributed to the CD signal from **RB** in chiral voids. For **RB** molecules, a pair of enantiomer with mirror-imaged axis chirality originated from the rotation of phenyl rings relative to the xanthene unit (Figure S51), whereas fast rotation of phenyl rings led to silent CD signals for pure **RB** (Figure 4e). The newly generated CD band suggested that **RB** molecules were accommodated in the chiral porous skeleton, and a pref-
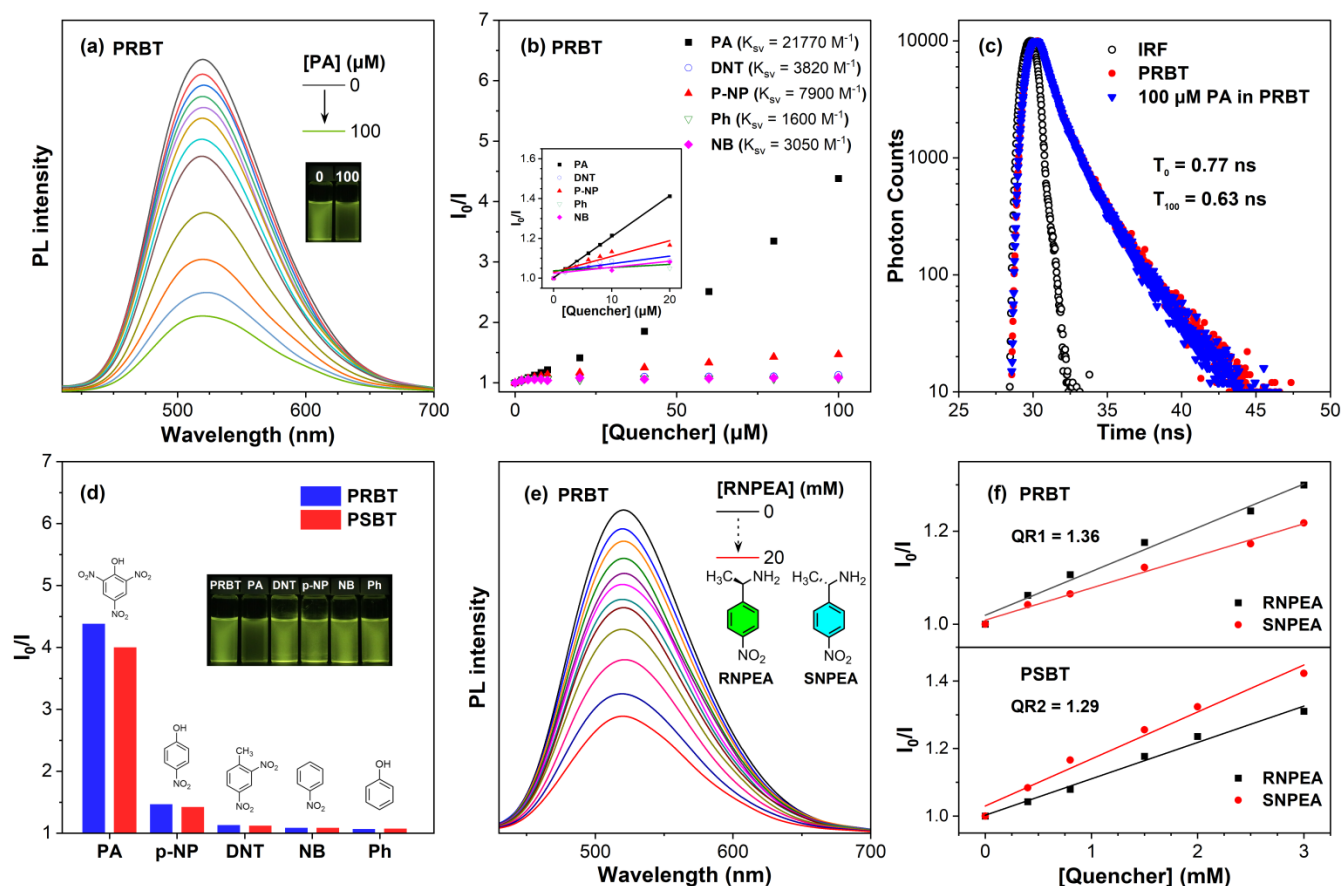
Figure 5. (a) PL spectra of chiral POP **PRBT** in MeOH in presence of PAs. (b) Dependence of PL intensity (I) on the concentration of PA and its analogues. (c) Luminescence lifetime decay of **PRBT** in MeOH in absence and presence of PAs (100 uM). (d) PL response of chiral POPs **PRBT** and **PSBT** with different analyst (100 μM). (e) PL spectra of chiral POP **PRBT** in MeOH in presence of chiral nitro-aromatics **RNPEA** and **SNPEA**. (f) Dependence of PL intensity (I) of **PRBT** and **PSBT** on the concentration of **RNPEA** and **SNPEA**. Excitation wavelength: 390 nm for **PRBT** and **PSBT**. Concentration: 10 uM for the repeating unit of chiral POPs.

erential chiral configuration was induced by chiral POPs. Time dependent DFT calculation (TD-DFT) of **RB** suggested that *P*-**RB** with clockwise helicity exhibited first negative Cotton effect at 460 nm, whereas *M*-**RB** with anti-clockwise rotation displayed positive CD signals (Figure S52). Based on the difference for CD spectra (ΔCD) of POPs in absence and presence of **RB** (Figure S50), **PRBT** skeleton would probably induce *M* helicity for **RB** whereas **RB** in **PSBT** adapted the *P*-helicity. To elucidate the binding models between chiral POPs and **RB**, the ¹H NMR spectra of **RBT-H** and **RB** had been recorded (Figure S53). The mixture of **RBT-H** and **RB** nearly displayed no changes relative to their component, which suggested that there was no host-guest interaction between the chiral macrocycle and **RB**. Considering the size of RB (around 1.2 nm in Figure S51), the dye guest was probably accommodated into the pores of chiral POPs rather than the internal voids of CCMs and further induced to adapt a preferential chirality in chiral porous skeletons.

Concerning the energy transfer and chirality transfer from chiral **POPs** to **RB**, the CPL spectra of their mixture were further measured. Obviously, the CPL emission for the mixture of chiral **POPs** and **RB** had gradually red-shifted to 608 nm, which was originated from **RB** (Figure 4f). However, the $|g_{lum}|$ value for these mixtures had gradually decreased to 0.46 × 10⁻³ (Figure S54 and Table S6). Compared to other amplified CPL system based on CPL-FRET, the amorphous nature of chiral POPs and non-uniform distribution and orientation of RB in the chiral porous skeleton probably contributed to the decreased $|g_{lum}|$ values.[54,55] However, these results had evidently confirmed the feasibility of color-tunable CPL system based on chiral luminescent POPs and chirality transfer from chiral porous hosts to guest dyes.

Enantioselective fluorescent sensing. Considering the porous structure of luminescent chiral POPs, their potential applications as fluorescent sensors were further studied with picric acid (PA) selected as the interested analyst. Along with the addition of PAs into the suspension of **PRBT** and **PSBT** in MeOH, the fluorescence intensity of chiral POPs gradually decreased with the increasing concentration of PA (Figure 5a). In addition, the PL titrations were also carried out for other nitro-aromatics and analogues (Figure S55-S56), including p-nitrophenol (p-NP), 2,4-dinitrotoluene (DNT), nitrobenzene (NB), and phenol (PN). By contrast, these analogues displayed remarkably lower quenching capability relative to PA (Figure 5b).

To confirm the underlying mechanism for this quenching process, PL lifetimes for these chiral POPs in MeOH were also measured in absence or presence of PA. As shown in Figure 5c, PL decay profiles revealed that the emission lifetimes of **PRBT** had gradually decreased from 0.77 ns in absence of PA to 0.63 ns in presence of PA (Figure 5c and S57). Therefore, we deduced that the quenching mechanism for these chiral POPs toward PA sensing was probably a dynamic quenching process without the formation of a stable non-fluorescent species between the chiral POPs with quencher molecules.[56,57] Based on the "Stern–Volmer" formalism, the quenching constant K_{SV} for **PRBT** and **PSBT** was calculated. The K_{SV} for PA and

PRBT was determined to be approximately 2.18 × 10⁴ M⁻¹ (Table S7), whereas the quenching constant for other analogues was one order lower (Figure 5d). Therefore, the luminescent chiral POPs had proven their potential as a promising sensor for explosive molecules with PA as the model compound.

Owing to the chiral porous skeleton and PA detection capability of **PRBT** and **PSBT**, enantioselective fluorescent sensing toward chiral nitro-aromatics were further explored. The enantiomers, (R)-1-(4-nitrophenyl)ethan-1-amine (**RNPEA**) and (S)-1-(4-nitrophenyl)ethan-1-amine (**SNPEA**), were selected as the interested compounds. As shown in Figure 5e, the PL intensity of **PRBT** in MeOH had gradually decreased with the addition of **RNPEA**, in which the emission decrease was obviously slower for **SNPEA** relative to its mirror-imaged analogue (Figure S58-S59). Similar to the detection of PAs, the luminescence lifetime of chiral POPs was also obviously attenuated suggesting a dynamic quenching process (Figure S60). The K_{sv} constants for **PRBT** were calculated to be 94.2 M⁻¹ and 70.4 M⁻¹ for R**NPEA** and **SNPEA** (Table S8), respectively, which afforded the quenching ratio [QR1 = $K_{sv(RNPEA)}/K_{sv(SNPEAl)}$] of 1.36. Additionally, the chiral POP **PSBT** displayed distinctively opposite selectivity, which suggested a similar quenching ratio [QR2 = $K_{sv(SNPEA)}/K_{sv(RNPEAl)}$] of 1.29 relative to its analogue. These quenching ratios were comparable with those reported BINOL-containing chiral porous polymers for enantio-sensing (Table S9).[11,58] And the enantio-selective sensing performance of this developed chiral macrocyclic POPs required to be further improved in the future.

CONCLUSIONS

We had demonstrated a modular synthetic approach toward chiral π-conjugated macrocyclic luminogens (**RBT** and **SBT**) integrating axis and helical chirality, whereas the chiral configuration was evidently confirmed by crystal analysis. After Yamamoto polymerization of the chiral macrocycles, a pair of chiral luminescent porous organic polymers with hierarchical porous structure was readily obtained and characterized. Owing to the existence of tetraarylethene units in the macrocycles, the CCMs all displayed aggregation-induced emission property and high emission efficiency in the solid state. These chiral small molecules and POPs also displayed mirror-imaged CD and CPL signals in solution, as nano-aggregates or suspension in MeOH, whereas the luminescence dissymmetry factor $|g_{lum}|$ was on the order of 10⁻³. Via energy transfer and chirality transfer from chiral POPs as host to guest dyes, the mixing of chiral POPs and Rhodamins had feasibly yielded CPL-active composites with tunable emission colors. These hierarchical chiral POPs were further utilized as fluorescence sensors for explosive molecules and chiral nitro-aromatics, which showed satisfactory enantioseletivity. These chiral conjugated macrocycles have established a modular approach toward chiral AIEgens, and the presented chiral macrocyclic POPs are the first two examples of conjugated POPs based on AIEgens with defined helicity. This work will promote the design and synthesis of more chiral porous polymers and

frameworks with intense emission and new functions based on the reported chiral AIEgens.

ASSOCIATED CONTENT

Supporting Information. Experimental details of synthesis and structural characterization, theoretical calculation results, single crystal data (CCDC 2408898 and 2408900), and supplementary figures. This material is available free of charge via the Internet at http://pubs.acs.org.

AUTHOR INFORMATION

Corresponding Author

* Yi Liu: liuyiacee@szu.edu.cn.

Author Contributions

#These authors contributed equally.

ACKNOWLEDGMENT

REFERENCES

[1] Kaur, P.; Hupp, J. T.; Nguyen, S. T. Porous Organic Polymers in Catalysis: Opportunities and Challenges. *ACS Catal.* **2011**, *1*, 819-835.

[2] Trewin, A.; Cooper, A. I. Porous Organic Polymers: Distinction from Disorder? *Angew. Chem. Int. Ed.* **2010**, *49*, 1533-1535.

[3] Chen, W.; Chen, P.; Zhang, G.; Xing, G.; Feng, Y.; Yang, Y.-W.; Chen, L. Macrocycle-Derived Hierarchical Porous Organic Polymers: Synthesis and Applications. *Chem. Soc. Rev.* **2021**, *50*, 11684-11714.

[4] Li, Z.; Yang, Y.-W. Conjugated Macrocycle Polymers. *Poly. Chem.* **2021**, *12*, 4613-4620.

[5] Li, Z.; Yang, Y.-W. Macrocycle-Based Porous Organic Polymers for Separation, Sensing, and Catalysis. *Adv. Mater.* **2022**, *34*, 2107401.

[6] Shetty, D.; Boutros, S.; Eskhan, A.; De Lena, A. M.; Skorjanc, T.; Asfari, Z.; Traboulsi, H.; Mazher, J.; Raya, J.; Banat, F.; Trabolsi, A. Thioether-Crown-Rich Calix[4]Arene Porous Polymer for Highly Efficient Removal of Mercury from Water. *ACS Appl. Mater. Interfaces* **2019**, *11*, 12898-12903.

[7] Dai, D.; Yang, J.; Zou, Y.-C.; Wu, J.-R.; Tan, L.-L.; Wang, Y.; Li, B.; Lu, T.; Wang, B.; Yang, Y.-W. Macrocyclic Arenes-Based Conjugated Macrocycle Polymers for Highly Selective Co2 Capture and Iodine Adsorption. *Angew. Chem. Int. Ed.* **2021**, *60*, 8967-8975.

[8] Skala, L. P.; Yang, A.; Klemes, M. J.; Xiao, L.; Dichtel, W. R. Resorcinarene Cavitand Polymers for the Remediation of Halomethanes and 1,4-Dioxane. *J. Am. Chem. Soc.* **2019**, *141*, 13315-13319.

[9] Li, Z.; Li, X.; Yang, Y.-W. Conjugated Macrocycle Polymer Nanoparticles with Alternating Pillarenes and Porphyrins as Struts and Cyclic Nodes. *Small* **2019**, *15*, 1805509.

[10] Zhang, Y.; Su, K.; Hong, Z.; Han, Z.; Yuan, D. Robust Cationic Calix[4]Arene Polymer as an Efficient Catalyst for Cycloaddition of Epoxides with Co2. *Ind. Eng. Chem. Res.* **2020**, *59*, 7247-7254.

[11] Yuan, C.; Fu, S.; Yang, K.; Hou, B.; Liu, Y.; Jiang, J.; Cui, Y. Crystalline C—C and C═C Bond-Linked Chiral Covalent Organic Frameworks. *J. Am. Chem. Soc.* **2021**, *143*, 369-381.

[12] Du, Y.; Yang, H.; Whiteley, J. M.; Wan, S.; Jin, Y.; Lee, S.-H.; Zhang, W. Ionic Covalent Organic Frameworks with Spiroborate Linkage. *Angew. Chem. Int. Ed.* **2016**, *55*, 1737-1741.

[13] Zhang, Y.; Duan, J.; Ma, D.; Li, P.; Li, S.; Li, H.; Zhou, J.; Ma, X.; Feng, X.; Wang, B. Three-Dimensional Anionic Cyclodextrin-Based Covalent Organic Frameworks. *Angew. Chem. Int. Ed.* **2017**, *56*, 16313-16317.

[14] Wang, Y.; Zhuo, S.; Hou, J.; Li, W.; Ji, Y. Construction of B-Cyclodextrin Covalent Organic Framework-Modified Chiral Stationary Phase for Chiral Separation. *ACS Appl. Mater. Interfaces* **2019**, *11*, 48363-48369.

[15] Kang, J.-Y.; Zhao, X.-B.; Shi, Y.-P. Azophenyl Calix[4]Arene Porous Organic Polymer for Extraction and Analysis of Triphenylmethane Dyes from Seafood. *ACS Appl. Mater. Interfaces* **2023**, *15*, 42981-42991.

[16] Li, X.; Li, Z.; Yang, Y.-W. Tetraphenylethylene-Interweaving Conjugated Macrocycle Polymer Materials as Two-Photon Fluorescence Sensors for Metal Ions and Organic Molecules. *Adv. Mater.* **2018**, *30*, 1800177.

[17] Wang, K.; Qi, D.; Li, Y.; Wang, T.; Liu, H.; Jiang, J. Tetrapyrrole Macrocycle Based Conjugated Two-Dimensional Mesoporous Polymers and Covalent Organic Frameworks: From Synthesis to Material Applications. *Coord. Chem. Rev.* **2019**, *378*, 188-206.

[18] Chen, M.; Li, H.; Liu, C.; Liu, J.; Feng, Y.; Wee, A. G. H.; Zhang, B. Porphyrin- and Porphyrinoid-Based Covalent Organic Frameworks (Cofs): From Design, Synthesis to Applications. *Coord. Chem. Rev.* **2021**, *435*, 213778.

[19] Haug, W. K.; Wolfson, E. R.; Morman, B. T.; Thomas, C. M.; McGrier, P. L. A Nickel-Doped Dehydrobenzoannulene-Based Two-Dimensional Covalent Organic Framework for the Reductive Cleavage of Inert Aryl C–S Bonds. *J. Am. Chem. Soc.* **2020**, *142*, 5521-5525.

[20] Yang, H.; Du, Y.; Wan, S.; Trahan, G. D.; Jin, Y.; Zhang, W. Mesoporous 2d Covalent Organic Frameworks Based on Shape-Persistent Arylene-Ethynylene Macrocycles. *Chem. Sci.* **2015**, *6*, 4049-4053.

[21] McKeown, N. B.; Gahnem, B.; Msayib, K. J.; Budd, P. M.; Tattershall, C. E.; Mahmood, K.; Tan, S.; Book, D.; Langmi, H. W.; Walton, A. Towards Polymer-Based Hydrogen Storage Materials: Engineering Ultramicroporous Cavities within Polymers of Intrinsic Microporosity. *Angew. Chem. Int. Ed.* **2006**, *45*, 1804-1807.

[22] Wang, Z.; Yan, S.; Cui, H.-C.; Cheng, G.; Ma, H.; Zhang, Q.-M.; Zhang, Q.-P.; Liu, J.-M.; Tan, B.; Zhang, C. Porous Organic Polymer from Aggregation-Induced Emission Macrocycle for White-Light Emission. *Macromolecules* **2018**, *51*, 7863-7871.

[23] Li, X.; Zhang, S.; Gao, J.; Wang, Z.; Yu, Q.; Zhao, Y.; Cheng, P.; Chen, Y.; Zhang, Z. The Recent Developments and Applications of Chiral Covalent Organic Frameworks. *Sci. Sin. Chim.* **2019**, *49*, 662-671.

[24] Han, X.; Yuan, C.; Hou, B.; Liu, L.; Li, H.; Liu, Y.; Cui, Y. Chiral Covalent Organic Frameworks: Design, Synthesis and Property. *Chem. Soc. Rev.* **2020**, *49*, 6248-6272.

[25] Wu, X.; Han, X.; Xu, Q.; Liu, Y.; Yuan, C.; Yang, S.; Liu, Y.; Jiang, J.; Cui, Y. Chiral Binol-Based Covalent Organic Frameworks for Enantioselective Sensing. *J. Am. Chem. Soc.* **2019**, *141*, 7081-7089.

[26] Zhang, S.; Zhou, J.; Li, H. Chiral Covalent Organic Framework Packed Nanochannel Membrane for Enantioseparation. *Angew. Chem. Int. Ed.* **2022**, *61*, e202204012.

[27] Hou, B.; Yang, S.; Yang, K.; Han, X.; Tang, X.; Liu, Y.; Jiang, J.; Cui, Y. Confinement-Driven Enantioselectivity in 3d

Porous Chiral Covalent Organic Frameworks. *Angew. Chem. Int. Ed.* **2021**, *60*, 6086-6093.

[28] Sun, B.; Kim, Y.; Wang, Y.; Wang, H.; Kim, J.; Liu, X.; Lee, M. Homochiral Porous Nanosheets for Enantiomer Sieving. *Nat. Mater.* **2018**, *17*, 599-604.

[29] Wang, L.-K.; Zhou, J.-J.; Lan, Y.-B.; Ding, S.-Y.; Yu, W.; Wang, W. Divergent Synthesis of Chiral Covalent Organic Frameworks. *Angew. Chem. Int. Ed.* **2019**, *58*, 9443-9447.

[30] Ma, H.-C.; Kan, J.-L.; Chen, G.-J.; Chen, C.-X.; Dong, Y.-B. Pd Nps-Loaded Homochiral Covalent Organic Framework for Heterogeneous Asymmetric Catalysis. *Chem. Mater.* **2017**, *29*, 6518-6524.

[31] Xu, H.; Gao, J.; Jiang, D. Stable, Crystalline, Porous, Covalent Organic Frameworks as a Platform for Chiral Organocatalysts. *Nat. Chem.* **2015**, *7*, 905-912.

[32] Sun, G.; Zhang, X.; Zheng, Z.; Zhang, Z.-Y.; Dong, M.; Sessler, J. L.; Li, C. Chiral Macrocycles for Enantioselective Recognition. *J. Am. Chem. Soc.* **2024**, *146*, 26233-26242.

[33] Zhang, G.-W.; Li, P.-F.; Meng, Z.; Wang, H.-X.; Han, Y.; Chen, C.-F. Triptycene-Based Chiral Macrocyclic Hosts for Highly Enantioselective Recognition of Chiral Guests Containing a Trimethylamino Group. *Angew. Chem. Int. Ed.* **2016**, *55*, 5304-5308.

[34] Yu, J.; Qi, D.; Li, J. Design, Synthesis and Applications of Responsive Macrocycles. *Commun. Chem.* **2020**, *3*, 189.

[35] Zhao, J.; Zeng, K.; Jin, T.; Dou, W.-T.; Yang, H.-B.; Xu, L. Circularly Polarized Luminescence in Macrocycles and Cages: Design, Preparation, and Application. *Coord. Chem. Rev.* **2024**, *502*, 215598.

[36] Ning, R.; Zhou, H.; Nie, S.-X.; Ao, Y.-F.; Wang, D.-X.; Wang, Q.-Q. Chiral Macrocycle-Enabled Counteranion Trapping for Boosting Highly Efficient and Enantioselective Catalysis. *Angew. Chem. Int. Ed.* **2020**, *59*, 10894-10898.

[37] Hu, M.; Feng, H.-T.; Yuan, Y.-X.; Zheng, Y.-S.; Tang, B. Z. Chiral Aiegens – Chiral Recognition, Cpl Materials and Other Chiral Applications. *Coord. Chem. Rev.* **2020**, *416*, 213329.

[38] Li, Y.; Liang, J.; Fu, S.; Huang, H.; Liu, S.; Wang, L.; Liu, Y. Full-Color-Tunable Chiral Aggregation-Induced Emission Fluorophores with Tailored Propeller Chirality and Their Circularly Polarized Luminescence. *Aggregate* **2024**, e613.

[39] Honda, T.; Ogata, D.; Tsurui, M.; Yoshida, S.; Sato, S.; Muraoka, T.; Kitagawa, Y.; Hasegawa, Y.; Yuasa, J.; Oguri, H. Rapid Synthesis of Chiral Figure-Eight Macrocycles Using a Preorganized Natural Product-Based Scaffold. *Angew. Chem. Int. Ed.* **2024**, *63*, e202318548.

[40] Penty, S. E.; Orton, G. R. F.; Black, D. J.; Pal, R.; Zwijnenburg, M. A.; Barendt, T. A. A Chirally Locked Bis-Perylene Diimide Macrocycle: Consequences for Chiral Self-Assembly and Circularly Polarized Luminescence. *J. Am. Chem. Soc.* **2024**, *146*, 5470-5479.

[41] Robert, A.; Naulet, G.; Bock, H.; Vanthuyne, N.; Jean, M.; Giorgi, M.; Carissan, Y.; Aroulanda, C.; Scalabre, A.; Pouget, E.; Durola, F.; Coquerel, Y. Cyclobishelicenes: Shape-Persistent Figure-Eight Aromatic Molecules with Promising Chiroptical Properties. *Chem. Eur. J* **2019**, *25*, 14364-14369.

[42] Zhao, W.-L.; Wang, Y.-F.; Wan, S.-P.; Lu, H.-Y.; Li, M.; Chen, C.-F. Chiral Thermally Activated Delayed Fluorescence-Active Macrocycles Displaying Efficient Circularly Polarized Electroluminescence. *CCS Chem.* **2022**, *4*, 3540-3548.

[43] Furlan, F.; Moreno-Naranjo, J. M.; Gasparini, N.; Feldmann, S.; Wade, J.; Fuchter, M. J. Chiral Materials and Mechanisms for Circularly Polarized Light-Emitting Diodes. *Nat. Photonics* **2024**, *18*, 658-668.

[44] Wang, Y.; Liu, X.; Li, H.; Liu, X.; Wang, L.; Liu, Y. Chiral Macrocyclic Aiegens from Binol and Tetraphenylethene Via Tailoring Chirality of Luminescent Molecular Propellers. *Chin. J. Chem.* **2022**, *40*, 2393-2399.

[45] Lee, T.; Peng, J. F. Photoluminescence and Crystal Structures of Chiro-Optical 1,1′-Bi-2-Naphthol Crystals and Their Inclusion Compounds with Dimethyl Sulfoxide. *Cryst. Growth Des.* **2010**, *10*, 3547-3554.

[46] Xu, Y.; Chen, L.; Guo, Z.; Nagai, A.; Jiang, D. Light-Emitting Conjugated Polymers with Microporous Network Architecture: Interweaving Scaffold Promotes Electronic Conjugation, Facilitates Exciton Migration, and Improves Luminescence. *J. Am. Chem. Soc.* **2011**, *133*, 17622-17625.

[47] Liu, Y.; Lin, F. X.; Feng, Y.; Liu, X.; Wang, L.; Yu, Z.-Q.; Tang, B. Z. Shape-Persistent Π-Conjugated Macrocycles with Aggregation-Induced Emission Property: Synthesis, Mechanofluorochromism, and Mercury(Ii) Detection. *ACS Appl. Mater. Interfaces* **2019**, *11*, 34232-34240.

[48] Lin, F.; Feng, Y.; Liu, X.; Wang, L.; Yu, Z.-Q.; Liu, Y. From Simple Katritzky Salts to Aiegens: Mechanochromic Luminescence and Heparin Detection. *Mater. Chem. Front.* **2020**, *4*, 1492-1499.

[49] Li, D.; Hu, R.; Guo, D.; Zang, Q.; Li, J.; Wang, Y.; Zheng, Y.-S.; Tang, B. Z.; Zhang, H. Diagnostic Absolute Configuration Determination of Tetraphenylethene Core-Based Chiral Aggregation-Induced Emission Compounds: Particular Fingerprint Bands in Comprehensive Chiroptical Spectroscopy. *J. Phys. Chem. C* **2017**, *121*, 20947-20954.

[50] Zhang, H.; Li, H.; Wang, J.; Sun, J.; Qin, A.; Tang, B. Z. Axial Chiral Aggregation-Induced Emission Luminogens with Aggregation-Annihilated Circular Dichroism Effect. *J. Mater. Chem. C* **2015**, *3*, 5162-5166.

[51] Hu, M.; Ye, F.-Y.; Du, C.; Wang, W.; Zhou, T.-T.; Gao, M.-L.; Liu, M.; Zheng, Y.-S. Tunable Circularly Polarized Luminescence from Single Crystal and Powder of the Simplest Tetraphenylethylene Helicate. *ACS Nano* **2021**, *15*, 16673-16682.

[52] Liang, J.; Fu, S.; Wu, Q.; Wang, P.; Liu, X.; Wang, L.; Liu, Y. Stimuli-Responsive Chiral Aggregation-Induced Emission Luminogens and Their Circularly Polarized Luminescence. *J. Mater. Chem. C* **2024**, *12*, 19140-19147.

[53] Du, C.; Zhu, X.; Yang, C.; Liu, M. Stacked Reticular Frame Boosted Circularly Polarized Luminescence of Chiral Covalent Organic Frameworks. *Angew. Chem. Int. Ed.* **2022**, *61*, e202113979.

[54] Yuan, Y.-X.; Jia, J.-H.; Song, Y.-P.; Ye, F.-Y.; Zheng, Y.-S.; Zang, S.-Q. Fluorescent Tpe Macrocycle Relayed Light-Harvesting System for Bright Customized-Color Circularly Polarized Luminescence. *J. Am. Chem. Soc.* **2022**, *144*, 5389-5399.

[55] Wu, Y.; Yan, C.; Li, X.-S.; You, L. H.; Yu, Z.-Q.; Wu, X.; Zheng, Z.; Liu, G.; Guo, Z.; Tian, H.; Zhu, W.-H. Circularly Polarized Fluorescence Resonance Energy Transfer (C-Fret) for Efficient Chirality Transmission within an Intermolecular System. *Angew. Chem. Int. Ed.* **2021**, *60*, 24549-24557.

[56] Liu, X.; Wang, Y.; Liu, X.; Liu, S.; Li, Y.; Wang, L.; Liu, Y. Dendritic Polyphenylene Aiegens: Fluorescence Detection of Explosives and Stimulus-Responsive Luminescence. *Poly. Chem.* **2022**, *13*, 6197-6204.

[57] Liu, X.; Lei, P.; Liu, X.; Li, Y.; Wang, Y.; Wang, L.; Zeng, Q.; Liu, Y. From Luminescent Π-Conjugated Macrocycles to Bridged Multi-Cyclic Π-Conjugated Polymers: Cyclic Topology, Aggregation-Induced Emission and Explosive Sensing. *Poly. Chem.* **2023**, *14*, 2979-2986.

[58] Valverde-González, A.; Borrallo-Aniceto, M. C.; Pintado-Sierra, M.; Sánchez, F.; Arnanz, A.; Boronat, M.; Iglesias, M. Binol-Containing Chiral Porous Polymers as Platforms for Enantiorecognition. *ACS Appl. Mater. Interfaces* **2022**, *14*, 53936-53946.
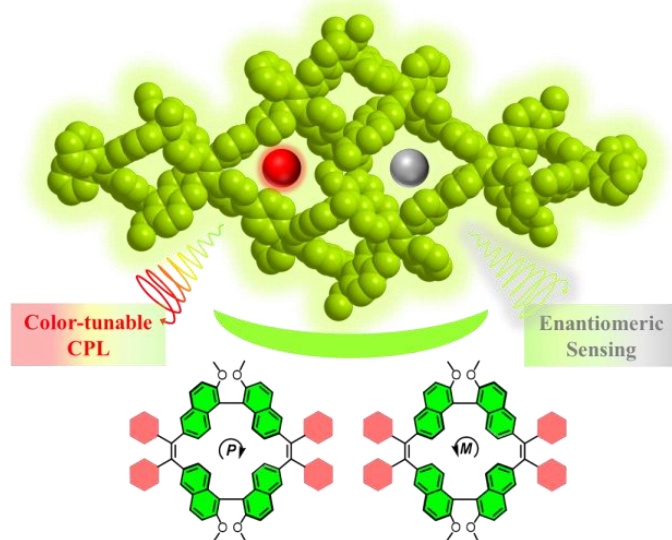

Table of Contents artwork